EUROFUSION WPHCD-PR(16) 16719

LG Garrigues et al.

Appropriate use of the Particle-In-Cell method for the simulation of negative ion extraction

Preprint of Paper to be submitted for publication in
Journal of Applied Physics

This work has been carried out within the framework of the EUROfusion Consortium and has received funding from the Euratom research and training programme 2014-2018 under grant agreement No 633053. The views and opinions expressed herein do not necessarily reflect those of the European Commission.

Appropriate use of the Particle-In-Cell method for the simulation of negative ion extraction

L. Garrigues[†], G. Fubiani, and J.P. Boeuf

LAPLACE, Université de Toulouse, CNRS, INPT, UPS, France

Abstract

The Particle-In-Cell Monte Carlo Collision (PIC MCC) method has been used by different authors in the last ten years to describe negative ion extraction in the context of neutral beam injection for fusion. Questionable results on the intensity and profile of the extracted negative ion beamlets have been presented in several recently published papers. Using a standard explicit PIC MCC method we show that these results are due to a non-compliance with the constraints of the numerical method (grid spacing, number of particles per cell) and to a non-physical generation of the simulated plasma. We discuss in detail the conditions of mesh convergence and plasma generation and show that the results can significantly deviate from the correct solution and lead to unphysical features when the constraints inherent to the method are not strictly fulfilled. Since the results presented in this paper have been obtained with careful validation of the method we propose them as benchmarks for future comparisons between different simulation codes for negative ion extraction.

[†] Electronic mail: laurent.garrigues@laplace.univ-tlse.fr

I. Introduction

A large variety of high power negative ion sources exists worldwide as a precursor for accelerator applications [1]. Neutral beam injection is an important means of plasma heating in magnetic fusion. It is successfully used in Tokamak machines [2], [3], and will operate in ITER [4] and future DEMO [5] reactors. A neutral beam injection (NBI) system is typically composed of a low-temperature plasma source where negative ions are generated and extracted, a system of polarized grids leading to the acceleration of negative ions to high energies (~ 1 MeV for ITER), a neutralizer where negative ions are converted in neutrals through collisions with ambient neutral gas, and a residual ion dump zone where electric (or magnetic) fields are used to deflect remaining charge species. Two low-temperature ITER prototype plasma sources have been constructed and are being tested at IPP Garching, BATMAN (Bavarian test machine for negative ions) [6-8], and ELISE (Extraction from a large source experiment) [9], at 1/8 and 1/2 of the machine size used for ITER, respectively.

In these sources a power on the order of 100 kW is inductively coupled to the plasma in a radiofrequency driver operating at 1 MHz in hydrogen (deuterium in fusion applications) under low pressure conditions (on the order of 0.3 Pa for the ITER source). The plasma diffuses in an expansion chamber separated from the extraction region by a magnetic filter. The role of the filter is to reduce the electron temperature in order to limit the destruction of negative ions by fast electrons. The extraction system downstream of the magnetic filter is composed of a positively biased plasma grid (PG) (at a potential close to floating conditions) and an extraction grid (EG) at a potential of about 10 kV above the chamber potential and placed at several mm from the PG. A deflection magnetic field whose role is to prevent or at least limit the co-extracted electron current is generated by permanent magnets placed inside the EG. To achieve the ITER negative ion current density requirements, the extraction area

will be 2000 cm^2 and the negative ion beam will consist in 1280 separated beamlets of diameter on the order of 1 cm emitted by each grid aperture [8], [10].

The volume production of negative ions by dissociative attachment to vibrationally excited molecules is not sufficient to reach the 55 A of negative ion current required for the ITER operation. To enhance negative ion production and current extraction, cesium is vaporized in the source and a thin layer of cesium covers the PG surface. As a consequence, the work function of the grid surface is lowered and negative ions are produced at the surface through the impingement of positive ions and neutral hydrogen atoms. A review detailing the mechanisms of negative ion production in volume and at the surface in the context of magnetic fusion is presented in Ref. [11]. At 100 kW and for a pressure of 0.4 Pa, the measured negative ion current density in BATMAN is less than 30 A/m^2 without cesium and reaches 150 A/m^2 when the source operates with cesium [6].

Modeling is important to better understand the physics of negative ion extraction and the parameters controlling the extracted current and beam optic. A number of simulation tools have been developed and validated and are available for the simulation of positive ion extraction from a plasma, but this is not the case for negative ion extraction. The simulation of negative ion extraction is more difficult for several reasons: 1) in extraction models for positive or negative ions the plasma density is a given parameter, but in the case of negative ion extraction, the density of negative ions in front of the plasma grid is an independent parameter that must be self-consistently determined and depends on surface as well as volume production and destruction mechanisms, 2) in the case of surface production of negative ions, space charge limitation of the emitted current is an issue and must be accurately described in the model, 3) the transport of negative ions from the surface to the extracting aperture is not a simple question (how long is the ion path from the surface to the aperture, what is the role of collisions?), 4) electron transport in the region around each aperture is extremely complex due

to their strong magnetization and to the complex magnetic field distribution (3D, non-axisymmetric problem, EXB effects?), 5) extraction models generally focus on a small region around each aperture, with periodic boundary conditions; in a negative ion source the presence of the magnetic filter makes it difficult to treat the small region around the aperture independently of the whole plasma source (questions of boundary conditions and plasma injection in the simulated domain).

During the last 10 years, several groups have developed different models of negative ion extraction based on the use of the Particle-In-Cell Monte Carlo Collisions (PIC MCC) method. The physics of negative ion extraction has been studied with one-dimensional models [12], [13], two-dimensional models where a flat aperture corresponding to an infinite slit is simulated (as sketched in Figure 1) [14-18], and three-dimensional models where a single cylindrical aperture is simulated [19-23]. The chamfered geometry of the plasma grid aperture, recommended for the ITER design, has been considered in some 3D models. This conical aperture geometry, with a larger diameter on the side of the plasma grid facing the plasma, is supposed to facilitate the transport of the surface emitted negative ions to the aperture.

The 3D PIC MCC simulations of Refs [19-23] led to the conclusion that only the inside edges of the chamfered grid aperture contribute to the extracted negative ion current because a large part of the negative ions emitted by the PG are reflected back to the surface due to the presence of a large potential well (virtual cathode formation and space charge limitation of the current extracted from the surface). To reach values of the extracted negative ion current consistent with the experiments, the authors of Ref. [19] had to assume extremely large values of the current density emitted by the surface (1800 A/m^2, while the reference values discussed in Ref. [24] are in the 600-700 A/m^2 range). Since only negative ions emitted at the edges of the chamfered aperture were extracted in these simulations, a high divergence of the ion beamlet was observed ("hollow beamlet"). Using these calculated distributions of the negative

extracted ion current as input in the modeling of the ion beam in the entire accelerator, the authors of Ref. [25] found that as much as 20 % of the power was lost on the accelerating grids. This is not consistent with experiments and certainly not acceptable for the accelerator of the ITER neutral beam injection system. The measurements show that the negative ion current can indeed be extracted with a beamlet divergence satisfying the requirements [6], [26-28]. The experiments also show (Refs [6], [27-28]) that a significant negative ion current can be extracted even for non-chamfered plasma grids, i.e. that a large amount of negative ions emitted by the flat surface of the PG facing the plasma can flow through the virtual cathode potential well and reach the grid aperture (in other words the depth of the potential well is not very large with respect to the temperature of the emitted ions).

As mentioned above some of the results from PIC MCC simulations published in the last few years are questionable and we suspect and demonstrate in this paper that these questionable results are due to a misuse of the PIC MCC method (see also the discussion in Ref. [29]). The goal of this paper is to show that the constraints inherent to the PIC MCC method must be strictly respected and that significant deviations from the correct solution, sometime leading to unphysical results can be obtained when these requirements are not fulfilled. We focus on two aspects of the simulation that in our opinion can explain the questionable results obtained in previous publications: 1) the influence of numerical parameters such as grid spacing, and the question of mesh convergence of the simulations. As explained in the book of Birdsall and Langdon [30, p. 26], it is important, in PIC simulations, to "show the invariance of results as the nonphysical computer parameters (Δt, Δx, number of particles by cell, number of grid points, etc.) are changed"; 2) the method of plasma generation in the simulated domain.

The question of plasma generation in the simulated domain is discussed in section II where we briefly review the methods that have been used to create and sustain the plasma in front of

the PG and we describe the method that we use in the present paper. In section III, we give a brief overview of the EP-PIC (Explicit Parallel-Particle-In-Cell) simulation code that we have developed and used in this paper; the numerical constraints associated are also presented. In section IV, we study the accuracy and mesh convergence of the PIC method and discuss the consequences of non-respecting the numerical constraints, in the context of negative ion extraction. We summarize the main results and present the perspectives of this work in section V.

II. Plasma injection method

There is an abundant literature on the use of PIC simulations for the description of the sheath at the interface between a plasma and a wall [31-36]. In a one-dimensional version of such model the wall is for example the right boundary of the simulation domain while the left boundary is in the quasineutral plasma. An important issue in these models is how the plasma is injected in the domain. This can be done by the generation of charged particles in a region on the left part of the domain, sufficiently far from the wall, or by injecting charged particle fluxes from the left boundary. Depending on the injection method, the potential at the left or right boundary are given or the potential difference between the boundaries is a result of the simulation (this should be the case when charge particle fluxes are imposed). In any case it is difficult to avoid the formation of a "numerical" sheath at the left boundary. If charged particles are simply absorbed at this boundary then the left boundary acts as a wall and a standard sheath develops in front of it. The properties of the plasma in front of the wall are supposed to be given so another issue is how to impose a given temperature of the plasma particles. The electrons need to be thermalized at a sufficient rate otherwise their temperature decreases because only high energy electrons are lost through the sheath (see below). The same issues arise in the simulation of ion extraction from a plasma. In the context of negative

ion extraction, the right wall is replaced by the system of plasma and extraction grids and the simulation is 2D or 3D with periodic boundary conditions along the PG.

The purpose of this section is to provide a brief and non-exhaustive review of the injection methods that have been used in the context of PIC simulations of negative ion extraction. The injection method is an important element of the simulation but is not always described in detail in published papers. In some papers the method is quite intricate, especially in cases where charged particle fluxes are imposed in the presence of a magnetic field. In Refs. [12], [14], [18], Taccogna *et al.* used a flux injection technique where appropriate flux distributions of charged particles (H^+, H_2^+, H_3^+, electrons and possibly H^-) are continuously injected through the left-boundary (LB) plane of the simulation domain. The initial distributions of charged particles are loaded according to a *shifted Maxwellian distribution* (see Appendix). Taccogna *et al.* use a refluxing process that consists in reflecting back all the particles crossing the LB plane and to sample three new velocity components according to a *Maxwellian distribution* (see Appendix) at the source temperature [31]. In the refluxing method, when one particle crosses the LB plane from the right to left direction (out of the domain), a "ghost" particle coming from left enters in the domain with the properties of the plasma source. This injection method has two main drawbacks: 1) due to the electron gyration in the magnetic field of the filter in front of the PG (B_F - see fig. 1), the injected electrons cross many times the LB plane, and 2) the re-injection of negative ions coming from the PG surface is questionable since many negative ions will be accelerated towards the upstream plasma source where they will be detached by high energetic electrons. In Poisson's equation, the normal electric field is fixed to 0 (Neumann boundary condition).

Another method for sustaining a quasineutral plasma in a PIC simulation is to inject particles in a given region of the simulation domain, upstream of the PG (see Refs. [13], [15-17], [19-23]). There are different ways of injecting particles in the volume of the simulation

domain. Wunderlich *et al.* start with an empty simulation domain and electrons and positive ions are injected continuously at the same, given rate and at a given, source position (point source) [13], as recommended in Refs [32-34].

In Refs [19-22], the method of injection is different and is such that the different charged particles are injected at different rates (which is in our opinion very questionable, as discussed below). In this method, equal numbers of negative charges and positive ions are loaded with a *Maxwellian distribution* in a fixed region of the simulation at the beginning of the simulation. This fixes the initial quasineutral plasma conditions (density and temperature). When one charged particle collides with the PG, EG or LB, the *same kind* of charged particle is re-injected at a random position in the source region in Refs [19-22]. Therefore the total number of electrons and the total number of positive ions stay constant during the simulation. When the energy of one incident electron impacting the PG is above a given secondary emission threshold, the incident electron is backscattered with new velocity components sampled from a *Maxwellian distribution* at a given temperature at the PG surface (to model secondary electron emission), otherwise, the incident electron is lost and a new electron is re-injected in the source region. This injection method is highly questionable, as said above, because the rate of generation of electrons and positive ions are different so current continuity is not satisfied. It is easy to see that this method is for example unable to describe the formation of a positive ion sheath in the simple case of an electron-positive ion plasma in front of a grounded wall. In a sheath the number (or the density) of electrons adjusts so that the electron and ion fluxes to the walls are identical (or result in a given, non-zero total current to the wall). The method of Refs [19-22] imposes an electron flux much larger than the ion flux to the wall and would lead to an unphysical description of the wall sheath (a comparison of this questionable injection method with a more physical one is discussed below and illustrated in Fig. 2). Since the method cannot describe the simple problem of a sheath in front of a wall, one can infer

that it can hardly properly describe the more complex problem of negative ion extraction by a system of plasma grid and extraction grid.

A simple and natural method of injection, which is used in the present paper, consists in loading a new electron-positive ion pair in the source region whenever one positive ion collides with the PG or LB [15-17] [23]. The number of electrons self-consistently adapts to ensure current continuity. This method is similar, for steady state problems, to the method where electron-ion pairs are generated at a given rate except that the ion density is imposed (and not the generation rate). Since the grid spacing is related to the plasma density (grid spacing on the order of the Debye length) it is more convenient to impose the plasma density than the generation rate of electron-ion pairs. In this method the potential of the left boundary can be fixed and the boundary can be supposed to be a sink for charged particles. In that case a sheath develops on the left boundary. This sheath is clearly artificial but has no consequence on the extraction physics. The only relevant parameter is the plasma potential that establishes in the simulation sufficiently far from the PG (and which depends on the potential applied on the different boundaries, LB, PG and EG). For given values of the PG and EG potentials, the potential applied on the left boundary controls the electron and positive ion currents flowing to the right boundary (PG and EG) just as the voltage bias applied to the PG controls these current in a real experiment. The important parameter, to be compared with experiments when the effect of this bias voltage is studied, is the difference between the plasma potential (not the LB potential) and the PG potential.

Another important issue concerns the use of an appropriate method to maintain the electron temperature in the injection region (and equal to the initial one). Injecting electrons in the source region at a given temperature is not sufficient to maintain a constant electron temperature in the plasma since only electrons with energy above the sheath potential are continuously lost to the walls [15]. The consequence (eg in the example above of a plasma

sheath in front of a wall in a non-magnetized electron-positive ion plasma) is that the electron temperature in the plasma will stay below the imposed temperature and that the plasma potential will also be below the expected one. To maintain the electron temperature in the source region equal to the initial electron temperature, an artificial "thermalization" mechanism must be used [13], [37]. This can be done as follows. In the source region, the velocity components of the electrons are replaced with new components taken from a *Maxwellian distribution* at a fixed temperature (T_{th} equal to T_e) at a given "thermalization frequency" ν_{th} (electrons that will be "thermalized" are randomly chosen at each time step as in a collision process). The thermalization frequency is chosen in such a way that electrons are on the average thermalized at least on time during their stay in the source region. One consequence of this "collisional thermalization" procedure is that it affects the transport across the magnetic field since it increases the effective momentum transfer frequency of the electrons.

To illustrate the effect of the plasma generation method we have compared PIC simulation results obtained with the two methods described above in the case of a simple one-dimensional (x direction, 32 mm length) collisionless non-magnetized plasma with grounded walls. The considered species are electrons (of mass m and temperature T_e = 2 eV) and H_2^+ ions (of mass M = 2 a.m.u. and temperature of 0.1 eV). The source injection region is between x = 5 mm and x = 27 mm. We use the mechanism of thermalization presented above to maintain an electron temperature of 2 eV. The initial plasma is neutral, with a density set to 1.2×10^{15} m^{-3}. The number of grid cells is fixed to 200 to resolve the Debye length. The plasma potential can be obtained analytically by writing that the current to the wall is zero, and is given by [38]:

$$V_p = \frac{kT_e}{2}\left[\ln\left(\frac{M}{2\pi m}\right) + 1\right] \qquad (1).$$

This gives a plasma potential of 7.4 V in our conditions. A comparison of time-averaged electric potential profile according to the two methods of plasma injection described above is shown in Fig. 2. In the injection method where an *electron-ion pair* is re-injected each time one ion collides with the grounded walls, the maximum of electric potential perfectly matches the analytical value. In the injection method where the *same kind* of charged particle is re-injected each time one electron or one ion hits the boundary, the time averaged potential in the center of the discharge is negative, which clearly corresponds to a non-physical situation with electron sheaths instead of ion sheaths in front of the walls!. Positive ions are confined in the center of the plasma while there is a large electron flux out of the plasma (and a large electron source in the source region). The simulations also show large oscillations of the electric potential in these conditions. We conclude that the method where a particle of the same type is re-injected each time one electron or one ion hits a boundary is clearly not appropriate to generate a plasma in a bounded system.

III. Description of the Explicit-Parallel Particle-In-Cell Model

A. Basic principles of the electrostatic PIC model

The EP-PIC (Explicit Parallel – PIC) model used in this paper is based on a standard 2D-3V (2 dimensions in space, 3 in velocity) PIC MCC method [30], [39] with parallelization. The simulation is performed on a 2D domain around a grid aperture (see figure 1). We consider three different charged species: electrons, positive ions (H_2^+) and negative ions (H^-). At each time step Δt, charged species are advanced under the actions of electric and magnetic forces obeying to the Newton-Lorentz laws using a leap-frog explicit scheme with the Boris algorithm [30], [39]. The Boris algorithm has the advantage of a minimum number of mathematical operations and only needs the storage of the particle properties at the previous

time step. The magnetic field **B** is imposed externally while the electric field **E** is calculated at each time step through Poisson's equation:

$$\nabla . \mathbf{E} = \frac{\rho}{\varepsilon_0} \quad (2),$$

where ε_0 is the vacuum permittivity and ρ is the net charge density ($\rho = \sum q_s n_s$, q_s and n_s being the charge and density of each charged particle species *s*). Eq. (2) can be rewritten for the electric potential ϕ using $\mathbf{E} = -\nabla\phi$, as

$$\Delta\Phi = -\frac{\rho}{\varepsilon_0} \quad (3).$$

Using a finite difference centered discretization on a cartesian (*i*, *j*) mesh with a uniform grid (Δx, Δy), Eq. (3) becomes

$$\frac{\phi_{i+1,j}-2\phi_{i,j}+\phi_{i-1,j}}{\Delta x^2} + \frac{\phi_{i,j+1}-2\phi_{i,j}+\phi_{i,j-1}}{\Delta y^2} = -\frac{\rho_{i,j}}{\varepsilon_0} \quad (4)$$

This five points elliptic equation is solved with the PARDISO (Parallel Sparse Direct Linear Solver) [40] subroutine included in the Intel®Math kernel Library (Intel®MKL). The two components of the electric field along the *x* and *y* directions of the domain are deduced from the potential with difference centered method:

$$E^x_{i,j} = -\frac{\phi_{i+1,j}-\phi_{i-1,j}}{2\Delta \mathrm{x}}; E^y_{i,j} = -\frac{\phi_{i,j+1}-\phi_{i,j-1}}{2\Delta \mathrm{y}} \quad (5).$$

A linear shape factor [30], [39] is used to calculate the charged particle densities on the grid from the particle positions, and for electric field interpolation in the integration of the particle trajectories.

Boundary conditions for the electric potential ϕ, are periodic in the *y* direction and are of the Dirichlet type at the LB, PG and EG (see Fig. 1). The normal components of the electric field at the LB, PG and EG boundaries cannot be calculated from Eq. (5). On the LB plane (*i* = 0), the axial electric field $E^x_{0,j}$ is obtained from a linear extrapolation of the axial electric field at forward points [41]:

$$E_{0,j}^{x} = 2E_{1/2,j}^{x} - E_{1,j}^{x} = \frac{3\phi_{0,j} - 4\phi_{1,j} + \phi_{2,j}}{2\Delta x} \quad (6).$$

The same approach is used for all the electric field components normal to the walls and LB plane.

B. Collision module

Collisions between negatively charged particles, electrons and negative ions with neutral atoms and molecules (*H* and H_2) are included through a Monte Carlo Collisions (MCC) module (the density of neutral species is fixed and uniform). Only the main collisional processes are considered (assuming constant cross-sections derived from Ref. [42], see Table 1): for H^- electron detachment and elastic collision with H_2, and charge exchange with *H*, for electrons elastic collision with H_2.

The probability of first collision of a given particle charged during a time step Δt is :

$$P = 1 - \exp[-\nu_{tot}\Delta t] \quad (7),$$

where ν_{tot} is the total collision frequency of the particle. For sufficiently small time steps, $\nu_{tot,p}\Delta t_c \ll 1$, one can write:

$$P \approx \nu_{tot}\Delta t \approx \sum_{m=1}^{2} n_g^m \sigma_{tot}^m(\varepsilon_r^m)\mathrm{v}_r^m \Delta t \quad (8),$$

The sum *m* indicates the contribution of collisions of H^- with *H* and H_2, n_g^m corresponds to the neutral gas density (*H* or H_2), ε_r^m and v_r^m are the relative kinetic energy and velocity between the consider charged particle and the neutral species. The velocity of the colliding neutral species is sampled from a *Maxwellian distribution* at the given gas temperature. The total cross section σ_{tot}^m is the sum of all the collisional processes *j*:

$$\sigma_{tot}^m\left(\varepsilon_{r,p}^m\right) = \sum_j \sigma_j^m\left(\varepsilon_r^m\right) \quad (9).$$

In practice, this method is simple but very time consuming because it requires at each time step the calculations of the probability of collisions that includes relative energy and velocity, and cross sections for all the collisional processes for all the particles of species concerned by

collisions. A more efficient method adapted from the so-called *null collision* technique [43] is employed in this study. In PIC models, the null collision technique consists in using a total collision frequency equal to the maximum collision frequency ν_{max} in space and energy. In the example chosen, one obtains:

$$\nu_{max} = \sum_{m=1}^{2} n_g^m \langle \sigma(\varepsilon) \mathrm{v} \rangle_{max}^m \quad (10).$$

The maximum of collision probability $P_{max} = \nu_{max} \Delta t_c$ [43], [44] is now independent of time and particle properties. For each species, the number N_c of particles that collides is chosen randomly in the list of particles according to $N_c = P_{max} N$ where N is the total number of particles of this type. Since $P_{max} \ll 1$, $N_c \ll N$ and a restricted number of particles experience collisions, the time passed in the MCC procedure is largely reduced. The procedure to determine the nature of the collision is detailed in Refs [44], [45]. By arbitrary overestimating the collision frequency, this method introduces fictitious or null collisions (of frequency $\nu_{null} = \nu_{max} - \nu_{tot}$) that are treated as a non-event in the sense that no real collision occurs for the particles when this process is selected. After real collisions, the new velocity components are calculated (assuming isotropic scattering angle) using standard methods (see eg Ref. [46]).

C. Simulation domain, magnetic field, and injection method

The two-dimensional computational domain, shown in figure 1, is rectangular (*x*-*y* plane) with dimensions L_x = 32 mm and L_y = 16 mm, in *x* and *y* directions, respectively. The PG (thickness of 2 mm with an aperture of 8 mm in the center) is positioned at a distance of 3.5 mm downstream of the EG. The chosen values correspond to the typical size of flat grid system used to model negative ion extraction in the literature. The external magnetic field is composed of the field from the magnetic filter and from the deflection magnets. The magnetic field of the filter (B_F – see figure 1) is perpendicular to the simulation domain (*z* direction) and is supposed to be uniform and equal to 75 G [19]. The deflection magnetic field B_D is in

the simulation domain and its components are given by the following analytical expressions [38]:

$$B_{Dx} = B_D \sin\left[\pi\left(y - L_{y/2}\right)/L_y\right] \exp\left[-\pi(L_x - x)/L_y\right] \quad (11)$$

$$B_{Dy} = B_D \cos\left[\pi\left(y - L_{y/2}\right)/L_y\right] \exp\left[-\pi(L_x - x)/L_y\right] \quad (12),$$

with $L_{y/2} = L_y/2$ and $B_D = 600$ G.

The method of plasma injection is discussed in detail in section II and is summarized here. At the beginning of the simulation, an equal number of electrons and positive ions (initial density n_0) are loaded with a *Maxwellian distribution* at a temperature of 2 eV, between $x = 0$ to $x = 26.5$ mm. In the x direction, when one positive ion collides with the PG or crosses the LB a new electron-positive ion pair is loaded with a uniform distribution in the source region located between $x = 1$ and $x = 3$ mm according to *Maxwellian distributions* at temperatures of 2 eV for both species. Negative ions and electrons reaching the PG, EG and passing the LB plane are eliminated from the system. Electrons in the source region are continuously thermalized at a frequency $\nu_{th} = 2\times10^9$ s^{-1}. When one electron is thermalized, its new velocity components are loaded from a *Maxwellian distribution* at the thermalization temperature T_{th} equal to the initial electron temperature. Periodic boundary conditions are used in the y direction. A particle exiting at $y > L_y$ (respectively < 0) returns at a new y position $y' = y - L_y$ (respectively $y + L_y$) with same velocity components. At each time step, a continuous negative ion current density is injected uniformly along the PG surface (at x=26.5 mm) facing the plasma in the direction $x < 0$ according to a *half Maxwellian distribution* at a temperature of 1 eV.

D. Parallelization and sorting technique

The simulations can be very time consuming for high plasma densities and parallelization of the PIC model is necessary to achieve reasonable computation times. The EP-PIC code combines a hybrid parallelization taking advantage of distributed memory machine (with the

message passing interface MPI library routines for communications) and shared memory (with OpenMP). The parallelization method is based on the particle decomposition technique where charged particles are equally distributed on each core. Poisson's equation is not parallelized and solved on one core. The total net charge on this core is calculated as the sum of the net charge computed on all the cores. The electric field solution is then broadcasted to all cores for the time integration of the charged particle trajectories in the particle pusher (detailed information on the parallelization techniques for PIC simulations can be found in Ref. [47]).

A sorting method allowing an efficient use of the cash memory is implemented to reduce the time spent in searching the stored particle coordinates [48]. This method, which consists in sorting the particles every few time steps according to their position on the grid, is very effective for 3D problems, but a beneficial effect has also been achieved for 2D calculations with a large number of grid points (a reduction of 50 % of the time spent in the particle pusher procedure can be obtained for 1000 × 1000 grid points and 40 particles per cell).

E. Numerical constraints associated with explicit PIC models

The implementation of an explicit PIC model is simple, but the method is subject to severe constraints [30], [38]. A first constraint is associated with the grid spacing, which must be on the order or smaller than the electron Debye length: $\Delta x \leq \lambda_{D,e}$ (where $\lambda_{D,e} = \sqrt{\varepsilon_0 T_e / e^2 n_e}$). A second constraint is related to the time step which must a fraction of the plasma period: $\Delta t < 0.2/\omega_{p,e}$ (where $\omega_{p,e} = \sqrt{e^2 n_e / m\varepsilon_0}$ is the electron plasma frequency) to ensure stability and accuracy. When these two constraints are satisfied the CFL condition is fulfilled for particles traveling at the thermal velocity: $\mathrm{v}_{e,th}\, \Delta t/\Delta x < 1$. The last constraint is linked to the statistical representation of the charged particle distributions with a given number of macro-particles. The number of charged particles per cell, N_P, must be large enough to avoid

numerical heating and we find that at least several tens of particles per cell must be used to reach a sufficient accuracy (this is discussed below).

Considering a plasma density on the order of 3×10^{17} m^{-3}, an electron temperature of 2 eV as measured 2 cm downstream of the PG [6], and using a grid spacing equal to the electron Debye length, one can calculate the number of grid points necessary to model a given region around the grid aperture. For example, a 3D simulation box of 25 mm × 20 mm × 20 mm, would require 3.5×10^9 grid cells and, for a typical number of 40 particles per cell, a total of 1.4×10^{11} particles in the domain. Reaching a steady state regime in these conditions requires tremendous computer resources.

To reduce the computational time, Mochalskyy *et al.* have performed calculations with larger values of $\Delta x/\lambda_{d,e}$ in the injection region, on the order of 5 to 6, and with only few particles per cell (and much less by Debye sphere) [19], [21], [22]. The justifications given by the authors is that since the plasma density significantly decreases from the injection region to the PG aperture, the grid spacing to Debye length ratio in this region becomes much smaller (on the order or smaller than 1) so that the simulation should be accurate enough in the plasma meniscus region around the grid aperture. An appropriate very small time step was used in the simulations of Mochalskyy *et al.* to respect the time constraints. We show in the results below that even if the grid spacing is on the order of the local Debye length in the meniscus region, the fact that the grid spacing is much larger than the Debye length upstream, in the source region, leads to strong errors in the results. In the calculations of Taccogna *et al.*, $\Delta x/\lambda_{d,e}$ varies from 2 for 2D simulations [14] to 6 for 3D simulations [20] and the time step is chosen to be close to the inverse of electron plasma frequency, as required. The number of particles per cell is still low.

In the simulations of Refs. [15-17], [23], the constraint $\Delta x \leq \lambda_{d,e}$ is respected but the dimensions of the grid aperture and simulation domain are scaled down by a factor of 30. The

scaling of the dimensions was accompanied with a scaling of the magnetic field strength and extraction voltage, as described in Ref. [17] but the collision frequency was not scaled.

In the present paper, in order to comply with the constrains on the grid spacing to Debye length ratio, we performed simulations for plasma densities lower than the real plasma densities in the extraction region of the ITER negative ion source. The extraction voltage is also lower than in the real conditions. A discussion on how these results could be extrapolated (scaled) to the real, higher plasma density conditions, is left for future publications. The purpose here is to study the accuracy of the simulations as a function of numerical parameters such as grid spacing and number of particles per cell, to analyze the convergence of the simulations with decreasing grid spacing, and to compare results obtained with and without respecting the numerical constraints imposed by the PIC method.

IV. Numerical convergence and consequences of not respecting the constraints of the PIC method

The simulations have been performed for an initial plasma density n_0 of 6×10^{16} m^{-3} (to be compared with 3×10^{17} m^{-3} in the real device) and a negative ion current density emitted at the walls J_{inj} reduced by the same factor and fixed to 120 A/m^2. The temperature of injection of the negative ions T_{H^-} is 1 eV. Performing simulations at this lower plasma density allows us to explore and accurately analyze the influence of $\Delta x/\lambda_{d,e}$ on the results in a large range of variations of this parameter. In all the calculations, the term Δx will be used for grid spacing (a uniform grid is used with $\Delta y \sim \Delta x$) and is defined as $\Delta x = L_x/N_x$, N_x being the number of grid points varying from 128 (Δx = 250 μm) to 1500 (Δx = 21.3 μm) in the calculations. When the ratio Δx is larger than $\lambda_{d,e}$, Δt is adapted to strictly resolve the time constraint described above. Because of the smaller plasma density the extraction voltage Φ_{EG} is also

reduced and fixed to 1 kV. The PG is grounded and the potential at LB is – 5V. The positive ion temperature is 2 eV. All the parameters used in the model are summarized in Table 2.

A. Plasma properties – Influence of the grid spacing

We have plotted in figs 3a and 3b the axial profiles of T_e, and of the electric potential V at y = 0 (i.e. in between two grid apertures) for a grid spacing varying from 21.3 μm ($\Delta x/\lambda_{d,e}$ ~ 0.8) to 250 μm ($\Delta x/\lambda_{d,e}$ ~ 6 in average). The source region is indicated on the figure. The initial number of electrons and positive ions is 40 per cell. In all the cases, as expected, the electron temperature is maintained at 2 eV in the source region where a thermalization process is used (see Fig. 3a). The electron temperature strongly increases to reach 10 eV for Δx = 250 μm, while it is almost uniform for $\Delta x \leq 31.2$ μm. This result is due to numerical-heating also called self-heating (proportional for collisionless plasma to $\left[\Delta x/\lambda_{d,e}\right]^2$ [30], [39]). It is artificial and non-physical and is a consequence of not resolving the Debye length. As a consequence, the electric potential V exhibits a maximum of 4 V (with very large fluctuations in time – not shown) for Δx = 250 μm, see figure 3b.

When the grid spacing is decreased, the electric potential and electron temperature profiles converge towards the same solution below $\Delta x \leq 31.2$ μm. The T_e profile is flat, around 2 eV, in the source region where electrons are thermalized and slightly decreases toward the PG. The potential on the left of the domain is around 1 V. The potential is relatively flat and decreases close to the PG at x = 26.5 mm, due to the formation of a virtual cathode resulting from space charge saturation of the emitted negative ion current. The depth of the virtual cathode passes from -3.5 V to -1.2 V for Δx varying between 250 μm and 21.3 μm. The virtual cathode tends to be largely overestimated when the constraint on grid spacing to Debye length ratio is not satisfied (leading to lower negative ion extraction from the emitting PG surface).

The formation of the virtual cathode can be clearly seen in figure 4, which shows the profiles of the charged particle densities along $y = 0$ in the same conditions. The virtual cathode is the result of a balance between positive and negative charges (mainly negative ions emitted from the surface) in front of the PG and it is essential, for efficient extraction of negative ions from the surface, that positive ions be present close to the surface, to balance the negative ion space charge. For large Δx, the unphysical potential profile associated with numerical heating prevents a large part of the positive ions injected in the source region with a temperature of 2 eV to reach the PG surface. The positive ion density is less than 10^{16} m^{-3} and is not sufficient to neutralize the density of emitted negative ions. This, in turn, enhances the space charge saturation and increases the depth of the virtual cathode potential well, leading to a decrease of the negative ion current extracted from the surface. We see clearly on these results that when the grid spacing is larger than the Debye length in the source region, the wrong potential profile due to numerical heating prevents positive ions to reach the PG surface and neutralizes the emitted flux of negative ions, leading to a strong reduction of the negative ion current extracted from the surface.

The results described above explain the very low negative ion current extracted from the flat part of the PG surface and the very large depth of the virtual cathode potential well obtained in several publications where the grid spacing constraint was not satisfied. In the work of Taccogna *et al*., for 2D [14], [18] and 3D (with flat and chamfered apertures) geometry [20], only 5 % to 25 % of the negative ions emitted by the PG are extracted. For a chamfered geometry, a virtual cathode with a 5 V depth was formed in front of the flat part of the PG in this reference [20]. Similar results were obtained by Mochalskyy *et al*. for a 3D chamfered geometry where the positive ion density close to the flat part of the PG was only on the order of 5×10^{15} m^{-3} and the depth of the virtual cathode was around 6 V [21]. The authors speculated that the presence in the plasma volume of cesium positive ions could

balance negative charges but a reasonable estimation density of the Cs^+ density (~ 10^{15} m^{-3}) is not sufficient to modify the virtual cathode potential [20], [22].

As Δx decreases in our simulations, the electric potential profile becomes more flat, allowing more positive ions to reach the PG and leading to a reduction of the depth of the virtual cathode potential and to an increase of the negative ion current extracted from the surface. As a result, the negative ion density passes from 5×10^{14} m^{-3} for Δx = 250 μm to 10^{16} m^{-3} for Δx = 21.3 μm. A close look at the densities in front of the PG reveals that an ion-ion plasma is formed. The electronegativity factor α, defined as the ratio between negative ion density and electron density reaches 200 for Δx = 21.3 μm close to the PG. Cavity ring-down spectroscopy measurements of the density of negative ions have been performed at 2 cm upstream the PG with and without cesiated surfaces [49]. At 0.3 Pa and for cesiated surfaces, results show that the H^- density averaged along the y direction varies between 5 and 7×10^{16} m^{-3} when RF power varies from 40 to 80 kW. Assuming a linear scaling of the plasma density, the negative ion density obtained with the PIC model would be extrapolated to about 5×10^{16} m^{-3} in the conditions of a real source. Note that the calculated negative ion density is an upper limit since we have fixed the LB potential to - 5V, which implies that practically no negative ion escapes through the left boundary, i.e. is lost to the bulk plasma (see the discussion in Ref. [29]).

The variations of $\Delta x/\lambda_{d,e}$ and $\Delta x/\lambda_{d,H^-}$ along the x direction at y = 0 are plotted in Fig. 5. For large grid spacing, a very high $\Delta x/\lambda_{d,e}$ ratio is obtained in the source region since the electron temperature is maintained to 2 eV and the electron density reaches 2.8×10^{17} m^{-3}. Downstream of the source region, due to numerical heating, $\Delta x/\lambda_{d,e}$ decreases to lower value ~ 2. We see in the figure that taking $\Delta x \leq 31.2$ μm leads to exactly satisfy the grid spacing requirements. Not that another reason that can explain the small negative ion current extracted from the surface when the grid spacing is too large is the fact that in order to properly

describe the positive ion-negative plasma close to the PG surface, it is necessary that the grid spacing resolves the ion Debye length next to the surface [29]. The plot of $\Delta x/\lambda_{d,H^-}$ along the x direction, on Fig. 5b is very interesting in this respect. We see that $\Delta x/\lambda_{d,H^-} \leq 1$ is respected in all the domain for $\Delta x \leq 31.2$. For larger values of the grid spacing $\Delta x/\lambda_{d,H^-}$ can become much larger than 1 in the vicinity of the PG surface, because of the large negative ion density in the virtual cathode region. This may also have consequences on the inaccuracy of the simulations in these conditions and on the limitation of the calculated extracted current.

B. Plasma properties - Influence of the number of particles per cell

We have also studied the convergence of the results as a function of the number of particles per cell when $\Delta x/\lambda_{d,e} \sim 1$. (This choice is identical to the number of particles per Debye sphere as $\Delta x \leq \lambda_{d,e}$). Fixing Δx = 31.2 μm, we varied the initial number of electrons and positive ions per cell N_p between 10 and 80. The electron temperature and electric potential profiles are plotted in figure 6. At the maximum of T_e a variation of 0.5 eV (and ~ 0.5 V for electric potential) is obtained when N_p increases from 10 to 80. The virtual cathode depth passes from 1.3 V to 1.2 V when N_p varies from 10 to 80. Electron temperature and electric potential profiles converge as soon as $N_p \geq 40$. The variations of space charge densities for the same conditions are shown in figure 7. When N_p increases, in correlation with the electric potential shape, the peak of densities of electrons and positive ions in the source region is reduced. The density of positive ions at the sheath edge is a bit reduced for N_p = 10, explaining the lower density of negative ions in the volume. We clearly see that using a number of particles per cell $N_p \leq 10$ as has been done in previous PIC simulation reported in the literature can lead to important inaccuracies and errors. Our calculations show that taking a number of initial electrons and positive ions equal to 40 is a good compromise between accuracy and computational cost.

C. Meniscus and beamlet profile – Influence of the grid spacing

The electric potential profile along the *y* direction close to the PG for different grid spacing is shown in figure 8. An almost flat potential ~ -3.5 V is obtained for Δx = 250 μm while V decreases from -1 V at x = 0 (respectively 16 mm) to -1.5 V at x = 4 mm (respectively 12 mm). This is due to the gradient along the *y* direction of the net positive charge coming from the plasma. We see in Fig. 8 that for different grid spacing respecting the constraint $\Delta x/\lambda_{d,e} \leq 1$, i.e. for $\Delta x \leq 31.2$ μm, the potential profiles along the PG are practically identical. The average virtual cathode depth $\phi_{v,c}$ along the hole surface deduced from the PIC simulations can be compared with the theoretical one $\phi_{v,th}$ that can be estimated assuming a *half Maxwellian distribution*, as a function of the negative ion current saturation (transported to the plasma) j_{sat} and the negative ion current emitted at the surface j_{em} (see, eg [24] in the case of a 1D problem):

$$\emptyset_{v,th} = T_b \ln(j_{sat}/j_{em}) \quad (13),$$

where T_b is the temperature of the negative ions injected at the PG (T_b=1 eV). The agreement between the potential $\phi_{v,c}$ deduced from the PIC simulation and this simple expression is relatively good since we obtain: $\phi_{v,c}$ ~ - 3 V and $\phi_{v,th}$ ~ -2.5 V for Δx = 250 μm, and $\phi_{v,c}$ ~ - 1.35 V and $\phi_{v,th}$ ~ - 1.64 V for Δx = 21.3 μm (the difference between theoretical and calculated values is on the order of 20 %).

Using too large grid spacing has also important consequences on the shape of the plasma meniscus around the aperture and on the profile of the extracted negative ion beamlet. This is illustrated in figure 9, which displays the two-dimensional distributions of the positive ion density (contours) and negative ion current (vectors) for Δx = 250 μm and Δx = 31.2 μm. The number of initial electrons and positive ions is equal to 40 in both cases. As expected, the positive ion density is everywhere significantly larger for Δx = 31.2 μm. In the aperture region, the effect of the large applied potential at the EG is clearly visible on the positive ion density

profile. Above a given line corresponding roughly to a H_2^+ density ~ 3×10^{14} m^{-3}, the positive ions are reflected back and the sheath is constituted of negative ions and a small fraction of electrons. The line at the interface between the quasineutral plasma and the negatively charged region is called the meniscus. The value of the extraction potential (fixed to 1 kV in this work) has been chosen to keep a convex shape of the meniscus in all the calculations. The penetration of the meniscus in the plasma is deeper (~ 1 mm) for larger grid spacing. A perfect match for perveance corresponding to a lowest beam divergence was not searched. (The effect of the extraction potential on the meniscus and its consequence on negative ion beam properties is discussed in Ref. 29).

Using or not a grid spacing resolving the electron Debye length has dramatic consequences on the space distribution of the negative ion current density as shown in Fig. 9a and in Fig. 10. In Fig. 9a, when the grid spacing is large, the effective surface where injected negative ions can be extracted is reduced to the edges of the PG because of the large virtual cathode potential (see Fig. 8). The negative ions emitted from this region see a large accelerating electric field in the transverse (*y*) direction, leading to a large component of the beam current density non-parallel to the axis, and to the formation of a halo. Similar results are reported in Refs. [20], [21] where a chamfered aperture geometry was considered and where the simulations where performed with grid spacing much larger than the Debye length. For grid spacing small enough to resolve the electron Debye length, the effective surface of the PG contributing to negative ion extraction is now the whole surface, the negative ion current is more uniformly distributed among the meniscus, and the negative ion beamlet shown in figure 9b is much better behaved, almost parallel to the *x* direction and with a less pronounced halo.

The negative ion current density distribution at the EG along the *y* direction is plotted in figure 10. The beam halo corresponding to the wings of the distributions, visible at y = 6 mm and y = 10 mm for Δx = 250 μm, is very pronounced when $\Delta x/\lambda_{d,e} > 1$ but disappears as

$\Delta x/\lambda_{d,e} \leq 1$. The current density profile converges satisfactorily to the same distribution as $\Delta x/\lambda_{d,e} \leq 1$, if the number of particle per cell is sufficient (the figure gives an estimate of the error made with a simulation of 10 particles per cell, compared with 40).

To estimate the quality of the beam, one can calculate the RMS of the beam divergence at the end of the accelerator $\theta_m = \sqrt{\langle\theta^2\rangle - \langle\theta\rangle^2}$, where $\theta = \tan^{-1}(\mathrm{v}_y/\mathrm{v}'_x)$, v'_x being the velocity at the end of the accelerator considering negative ions at 1 MeV. The brackets indicate mean values taken on a sampling of 10 000 test particles. Calculations for Δx = 250 μm indicate a poor quality of the beam with θ_m ~ 10 mrad, while at Δx = 31.2 μm with N_p = 40, a better quality is achieved since θ_m ~ 6.7 mrad and consistent with ITER requirements [50].

V. Concluding remarks

A number of papers reporting the modeling of negative ion extraction for NBI, based on PIC MCC simulations, have been published in the last 10 years. The results described in some of these papers are questionable and the study reported in the present article tends to demonstrate that these questionable results are due to an inappropriate use of the PIC MCC method, i.e. under conditions where the accuracy requirements of the method were not fulfilled (and in some cases where the method of generation of the plasma in the simulation was violating current continuity).

We have provided a detailed and systematic analysis of the influence on the results of the grid spacing and on the number of particles per cell in the simulations.

Results show that when requirements of the PIC method are not fulfilled meaning $\Delta x/\lambda_{d,e} > 1$ and the initial number of particles in the system is under a certain limit, self-heating (or numerical heating) develops and leads to strong errors in the final results. The unphysical distribution of the plasma potential for large grid spacing prevents the positive

ions from reaching the PG surface and neutralizing the emitted negative ions. In these conditions an excessively large virtual cathode develops and negative ions are reflected back to the PG surface. This has strong consequences of the intensity and profile of the extracted beamlet: the extracted current is too small and the beamlet presents a strong divergence and large halo because negative ions are extracted only form the edges of the grid aperture. The results obtained in our simulations when using a large grid spacing are very similar to those reported in published simulation results where the constraints on the grid spacing inherent to a PIC simulation were not respected. When the constraint $\Delta x/\lambda_{d,e} \leq 1$ is respected and if a sufficient number of particles per cell (40 or more) is used in the simulation the numerical heating disappears and mesh convergence is achieved. The electric potential profile from the plasma to the grid surface is almost flat and allowing more positive ions to reach the PG. The depth of virtual cathode is consequently reduced and more negative ions coming from the whole PG surface can overcome the potential barrier and be later extracted through the grid aperture. The negative ion beamlet profile in these conditions is collimated and more conform to the expected profile.

The necessity to resolve the electron Debye length and to use a minimum of few tens of particles per cell makes the simulations for practical negative ion source conditions very time consuming in 2D and practically impossible in 3D. The results presented in this paper have been obtained for plasma density (and extraction voltage) lower than in the real source to allow a systematic parametric study of the influence of the numerical parameters, but the conclusions concerning the necessity to comply with the constraints inherent to PIC method can obviously be extrapolated to higher plasma densities.

Since the accuracy and the convergence of the results have been carefully checked and that the conditions of the simulations have been clearly described in this work, we consider that

the results presented here can be used for future benchmarks and comparisons between different simulation tools.

Acknowledgments

This work has been carried out within the framework of the EUROfusion Consortium and has received funding from the European Union's Horizon 2020 research and innovation programme under grant agreement number 633053. The views and opinions expressed herein do not necessarily reflect those of the European Commission. Support from CEA and from the French Fédération de Recherche sur la Fusion Magnétique is acknowledged. This work was granted access to the HPC resources of CALMIP supercomputing centre under the allocation 2013-P1125. The authors want to thank A. Simonin from CEA Cadarache for his support.

Appendix

We detail in this Appendix the different manners to load particle velocities in the system according to the different situations encountered or discussed in this work. The particle is characterized by its temperature T_j, charge q_j, and mass m_j. For a *Maxwellian distribution*, each components of the velocity has to be sampled according to a Gaussian probability distribution (e. g. for v_x component):

$$p(v_x) = \frac{1}{\sqrt{\pi} v_T} \exp\left[-\frac{v_x^2}{v_T^2}\right], -\infty < v_x < +\infty \quad \text{(A1)},$$

where $v_T = \sqrt{2 q_j T_j / m_j}$ is the thermal velocity. Same sampling has to be repeated for v_y and v_z components. Using 4 random numbers R_1 to R_4 generated between 0 and 1, one obtains:

$$v_x = v_T \sqrt{-\ln R_1} \cos(2\pi R_2) \quad \text{(A2)}$$

$$v_y = v_T \sqrt{-\ln R_1} \sin(2\pi R_2) \quad \text{(A3)}$$

$$v_z = v_T \sqrt{-\ln R_3} \cos(2\pi R_4) \quad \text{(A4)}.$$

The v_z' velocity is also calculated at the same time and saved in memory:

$$v_z' = v_T \sqrt{-\ln R_3} \sin(2\pi R_4) \quad \text{(A5)}.$$

Next time, to determine v_x' and v_y' only 2 random numbers will be necessary (and the time after again 4 random numbers).

To introduce a flux of particles from a wall surface as negative ions from the PG, a *half Maxwellian distribution* must be used. Let be *x* the direction of injection, the probability distribution obeys to the following law:

$$p(v_x) = \frac{2}{v_T} v_x \exp\left[-\frac{v_x^2}{v_T^2}\right], 0 < v_x < +\infty \quad \text{(A6)}.$$

The v_x component can be determined with one random number R_5:

$$v_x = v_T \sqrt{-\ln R_5} \quad \text{(A7)},$$

and v_y and v_z components are computed using Eqs. (A3) and (A4).

The last situation concerns the introduction a flux of particles from a non-physical surface like an open boundary to model a semi-infinite plasma. Let call *x* the direction of injection, the probability distribution can be sampled from a *shifted Maxwellian distribution*:

$$p(\mathrm{v}_x) = \frac{2}{\mathrm{v}_T}\mathrm{v}_x \exp\left[-\frac{(\mathrm{v}_x-\mathrm{u}_x)^2}{\mathrm{v}_T^2}\right], 0 < \mathrm{v}_x < +\infty \qquad \text{(A8)},$$

where u_x is related to a mean velocity consistent with particle velocities in the domain closed to the boundary. A direct sampling of v_x is impossible, Refs [51], [52] propose appropriate methods to sample v_x. The v_y and v_z components are simply obtained according to Eqs. (A3), (A4). An artificial sheath region is formed close to the open-boundary due to the injection of a distribution assuredly different from distribution in the domain where particles undergo collisions [31]. To reduce this effect, a method presented by Gozadinos *et al*. [35] is based on the adjustment of flux and local electric field iteratively fixing u_x equal to Bohm velocity. Hagelaar [51] prefers to self-consistently adjust u_x as a function of number of particles entering and leaving the domain.

References

[1] D. P. Moehs, J. Peters, and J. Sherman, IEEE Trans. Plasma Sci. **33**, 1786 (2005).

[2] M. L. Mayoral *et al*., Nucl. Fusion **54**, 033002 (2014).

[3] N. Umeda *et al*., Nucl. Fusion **43**, 522 (2003).

[4] R. S. Hemsworth, A. Tanga, and V. Antoni, Rev. Sci. Instrum. **79**, 02C109 (2008).

[5] A. Simonin *et al*., Nucl. Fusion **55**, 123020 (2015).

[6] E. Speth *et al*., Nucl. Fusion **46**, S220 (2006).

[7] R. S. Hemsworth *et al*., Nucl. Fusion **49**, 045006 (2009).

[8] U. Fantz *et al*., Plasma Phys. Control. Fusion **49**, B563 (2007).

[9] P. Frantzen *et al*., Fusion Eng. Des. **88**, 3132 (2013).

[10] M. Kashigawi *et al*., Rev. Sci. Instrum. **85**, 02B113 (2010).

[11] M. Bacal and M. Wada, Appl. Phys. Rev. **2**, 021305 (2015).

[12] F. Taccogna, R. Schneider, S. Longo, and M. Capitelli, Phys. Plasmas **15**, 103502 (2008).

[13] D. Wünderlich, R. Gutser, and U. Fantz, Plasma Sources Sci. Technol. **18**, 045031 (2009).

[14] F. Taccogna, M. Minelli, S. Longo, M. Capitelli, and R. Schneider, Phys. Plasmas **17**, 063502 (2010).

[15] S. Kuppel, D. Matsushita, A. Hatayama, and M. Bacal, J. Appl. Phys. **109**, 013305 (2011).

[16] K. Miyamoto, S. Okuda, and A. Hatayama, Appl. Phys. Let. **100**, 233507 (2012).

[17] K. Miyamoto, S. Okuda, S. Nishioka, and A. Hatayama, J. Appl. Phys. **114**, 103302 (2013).

[18] F. Taccogna, M. Minelli, P. Diomede, S. Longo, M. Capitelli, and R. Schneider, Plasma Sources Sci. Technol. **20**, 024009 (2011).

[19] S. Mochalskyy, A. F. Lifschitz, and T. Minea, J. Appl. Phys. **111**, 113303 (2012).

[20] F. Taccogna, M. Minelli, and S. Longo, Plasma Sources Sci. Technol. **22**, 045019 (2013).

[21] S. Mochalskyy, D. Wünderlich, B. Ruf, U. Fantz, P. Franzen, and T. Minea, Plasma Phys. Control. Fusion **56**, 105001 (2014).

[22] S. Mochalskyy, D. Wünderlich, U. Fantz, P. Franzen, and T. Minea, Nucl. Fusion **55**, 033011 (2015).

[23] S. Nishioka, I. Goto, K. Miyamoto, A. Hatayama, and A. Fukano, J. Appl. Phys. **119**, 023302 (2016).

[24] R. McAdams, A. J. T. Holmes, D. B. King, and E. Surrey, Plasma Sources Sci. Technol. **20**, 035023 (2011).

[25] A. Revel, S. Mochalskyy, L. Caillault, A. Lifschitz, and T. Minea, Nucl. Fusion **53**, 073027 (2013).

[26] R. S. Hemsworth *et al*., Nucl. Fusion **49**, 045006 (2009).

[27] Yu. I. Belchenko *et al*., Rev. Sci. Instrum. **75**, 1726 (2004).

[28] M. Kashigawi *et al*., Rev. Sci. Instrum. **85**, 02B320 (2014).

[29] J. P. Boeuf, G. Fubiani, and L. Garrigues, Plasma Sources Sci. Technol. **25**, 045010 (2016).

[30] C. K. Birdsall and A. B. Langdon, *Plasma Physics Via Computer Simulation* (IOP Publishing, New York, 2005).

[31] L. A. Schwager and C. K. Birdsall, Phys. Fluids B **2**, 1057 (1990).

[32] R. J. Procassini, C. K. Birdsall, and E. C. Morse, Phys. Fluids B **2**, 3191 (1990).

[33] K. Theilhaber and C. K. Birdsall, Phys. Fluids B **1**, 2244 (1989).

[34] R. J. Procassini, and C. K. Birdsall, Phys. Fluids B **3**, 1876 (1991).

[35] G. Gozadinos, D. Vender, and M. M. Turner, J. Comput. Phys. **172**, 348 (2001).

[36] L. Jolivet and J. F. Roussel, IEEE Trans. Plasma. Sci. **30**, 318 (2002).

[37] A. Froese, T. Takuzika, and M. Yagi, Contrib. Plasma Phys. **50**, 273 (2010).

[38] M. A. Lieberman, and A. J. Lichtenberg, *Principles of Plasma Discharges and Materials Processing* (New York, Wiley Interscience, 2005).

[39] R. W. Hockney and J. W. Eastwood, Computer Simulation Using Particles (Adam Hilger, New York, 1988).

[40] C. Petra, O. Schenk, M. Lubin, and K. Gaertner, *SIAM Journal on Scientific Computing* **36**, C139 (2014).

[41] C. Hirsch, *Numerical Computation of Internal and External Flows: Fundamentals of Computational Fluid Dynamics* (Elsevier, BH, 2007).

[42] R. K. Janev, D. Reiter, and U. Samm, *Collision Processes in Low-Temperature Hydrogen Plasmas*, Tech. Rep. 4105 (FZ-Juelich, 2003).

[43] J. P. Boeuf and E. Marode, J. Phys. D: Appl. Phys. **15,** 2169 (1982).

[44] V. Vahedi and M. Surendra, Comput. Phys. Commun. **87,** 179 (1995).

[45] J. P. Verboncoeur, Plasma Phys. Control. Fusion **47,** A231 (2005).

[46] G. Fubiani and J. P. Boeuf, Phys. Plasmas **20**, 113511 (2013).

[47] K. Germaschewski, W. Fox, S. Abbott, N. Ahmadi, K. Maynard, L. Wang, H. Ruhl, and A. Bhattacharjee, J. Comput. Phys. **318**, 305 (2016).

[48] K. J. Bowers, J. Comput. Phys. **173**, 393 (2001).

[49] M. Berger, U. Fantz, S. Christ-Koch, and NNBI Team, Plasma Sources Sci. Technol. **18,** 025004 (2009).

[50] L. Svensson, D. Boilson, H. P. L. de Esch, R. S. Hemsworth, and A. Krylov, Nucl. Fusion **46**, S369 (2006).

[51] G. J. M. Hagelaar, *Modeling Methods for Low Temperature Plasmas*, Habilitation à Diriger des Recherches, Toulouse, France, 2008.

[52] G. A. Bird, *Molecular Gas Dynamics and the Direct Simulation of Gas Flows* (Oxford University Press, Oxford, 1994).

Table 1. List of collisions in the volume. Cross sections are derived from Ref. [41] and collision frequencies are calculated for mean velocity.

Reactions	Process	Cross sections (m^2)	Frequency (s^{-1})
Electron atom elastic collision	$e + H_2 \rightarrow e + H_2$	1.4×10^{-19}	5×10^{6}
Charge exchange with H	$H^- + H \rightarrow H + H^-$	1.3×10^{-18}	3×10^{5}
Electron detachment with H_2	$H^- + H_2 \rightarrow e + H_2$	6.2×10^{-20}	5×10^{4}
Elastic collision with H_2	$H^- + H_2 \rightarrow H^- + H_2$	6.2×10^{-20}	5×10^{4}

Table 2. Input data used for the simulation

Physical parameters	Symbol	Value	Units
Initial plasma density/Gas densities	$n_0/n_{H_2}/n_H$	$6\times10^{16}/4\times10^{19}/1\times10^{19}$	m^{-3}
Initial temperature	$T_e/T_{H_2^+}/T_{H^-}/T_{H_2}/T_H$	2/2/1/0.1/1	eV
Thermalization frequency	ν_{th}	2×10^{9}	s^{-1}
Thermalization temperature	T_{th}	2	eV
Negative ion current density	J_{inj}	120	A/m^2
Applied potential	$\Phi_{LB}/\Phi_{PG}/\Phi_{EG}$	-5/0/1000	V
Deflection/filter magnetic field	B_D/B_F	600/75	G
Length in *x*/*y* direction	L_x/L_y	32/16	mm

Figure captions

Figure 1: schematic view of the simulation domain. Positions are indicated in mm. The grey region is the source region.

Figure 2: Comparison of electric potential profile for the two methods of plasma injection (see text).

Figure 3: profiles along the *x* direction at *y* = 0 for grid spacing varying from 21.3 μm to 250 μm of (a) electron temperature T_e and (b) electric potential V. The initial number of electrons and positive ions is 40 per cell. The source region is also presented.

Figure 4: profiles along the *x* direction at *y* = 0 for a grid spacing of 31.2 and 250 μm of (a) electron, (b) H_2^+, (c) H^- densities (in log scale), and (d) close to PG for a grid spacing of 31.2 μm. Same conditions as in figure 3.

Figure 5: profiles along the *x* direction at *y* = 0 of ratio of grid spacing to (a) electron Debye length, (b) H^- Debye length. Same conditions as in figure 3.

Figure 6: profiles along the *x* direction at *y* = 0 varying the initial number of electrons and positive ions N_p between 10 and 80 of (a) electron temperature T_e and (b) electric potential V. The grid spacing Δx = 31.2 μm. The source region is also presented.

Figure 7: profiles along the x direction at $y = 0$ varying the initial number of electrons and positive ions N_p between 10 and 80 of (a) electron, (b) H_2^+ and (c) H^- densities. Same conditions as in figure 6.

Figure 8: profiles of electric potential V along the y direction close to the PG for grid spacing varying from 21.3 μm to 250 μm. The initial number of electrons and positive ions is 40 per cell.

Figure 9: two-dimensional profiles of positive ion density (contour plot, log scale, maximum of 4×10^{16} m^{-3}) and negative ion current (vector plot) for (a) $\Delta x = 250$ μm and (b) $\Delta x = 31.2$ μm. The initial number of electrons and positive ions is 40 per cell.

Figure 10: Negative ion current density distribution at the EG along the y direction for varying grid spacing and initial number of electrons and positive ions per cell.

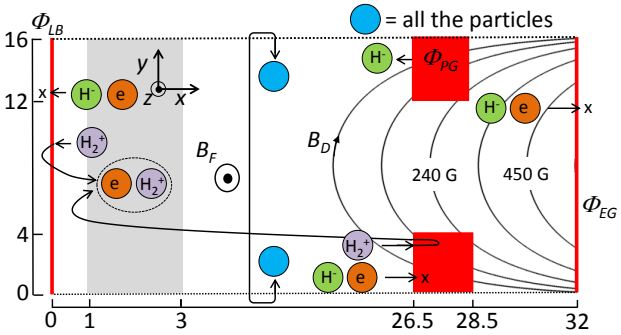
= all the particles
Φ_{LB}
Φ_{PG}
Φ_{EG}
B_F
B_D
240 G
450 G
16
12
4
0
0
1
3
26.5
28.5
32
x
y
z

Figure 1.

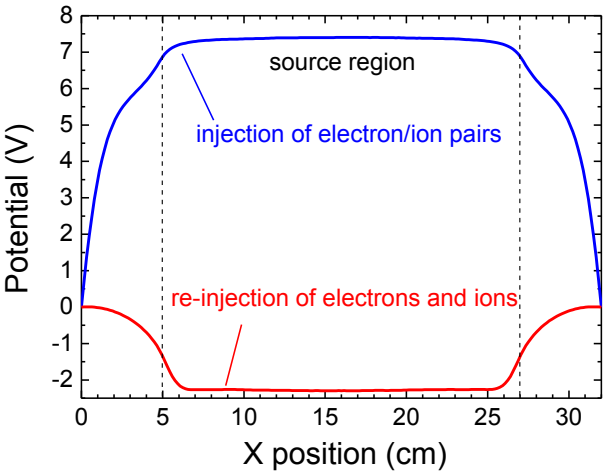
source region
injection of electron/ion pairs
re-injection of electrons and ions
Potential (V)
X position (cm)
8
7
6
5
4
3
2
1
0
-1
-2
0
5
10
15
20
25
30

Figure 2.

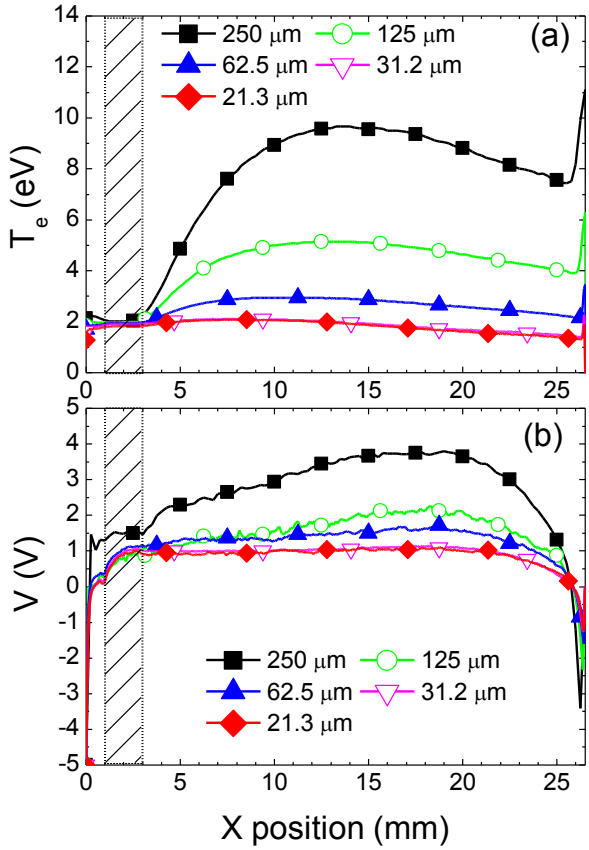

Figure 3.

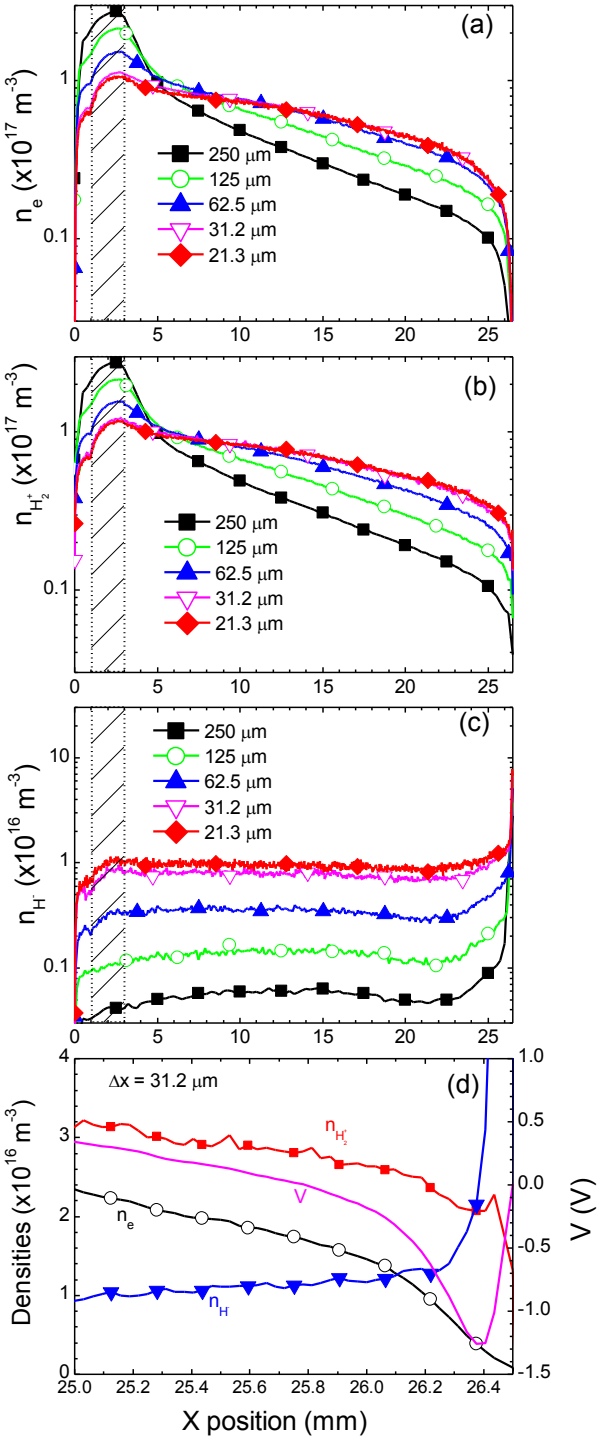
(a)
250 μm
125 μm
62.5 μm
31.2 μm
21.3 μm
(b)
(c)
(d)
Δx = 31.2 μm
V
X position (mm)
V (V)

Figure 4.

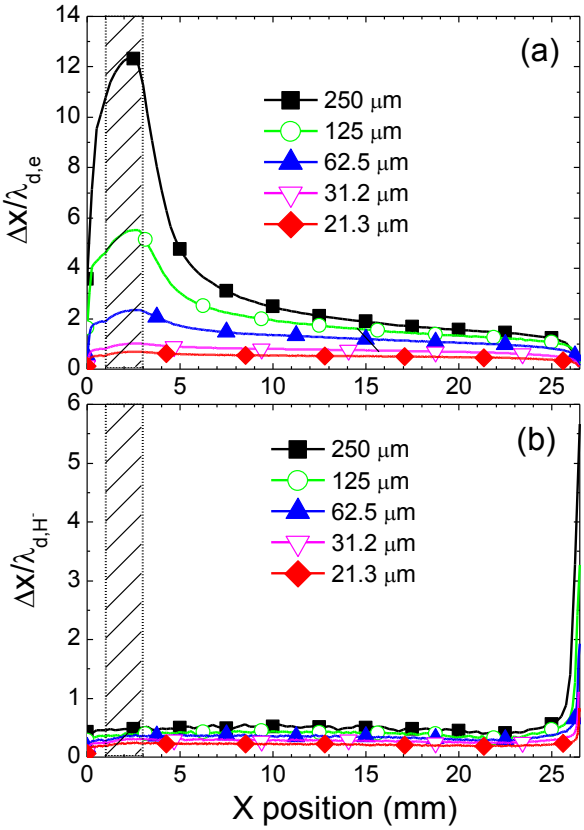
(a)
250 μm
125 μm
62.5 μm
31.2 μm
21.3 μm
Δx/λd,e
(b)
250 μm
125 μm
62.5 μm
31.2 μm
21.3 μm
Δx/λd,H-
X position (mm)

Figure 5.

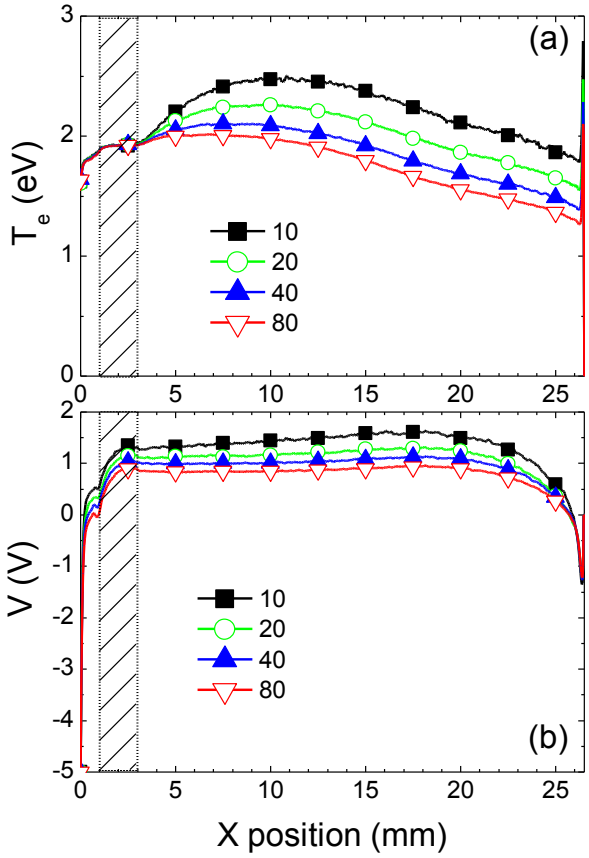

Figure 6.

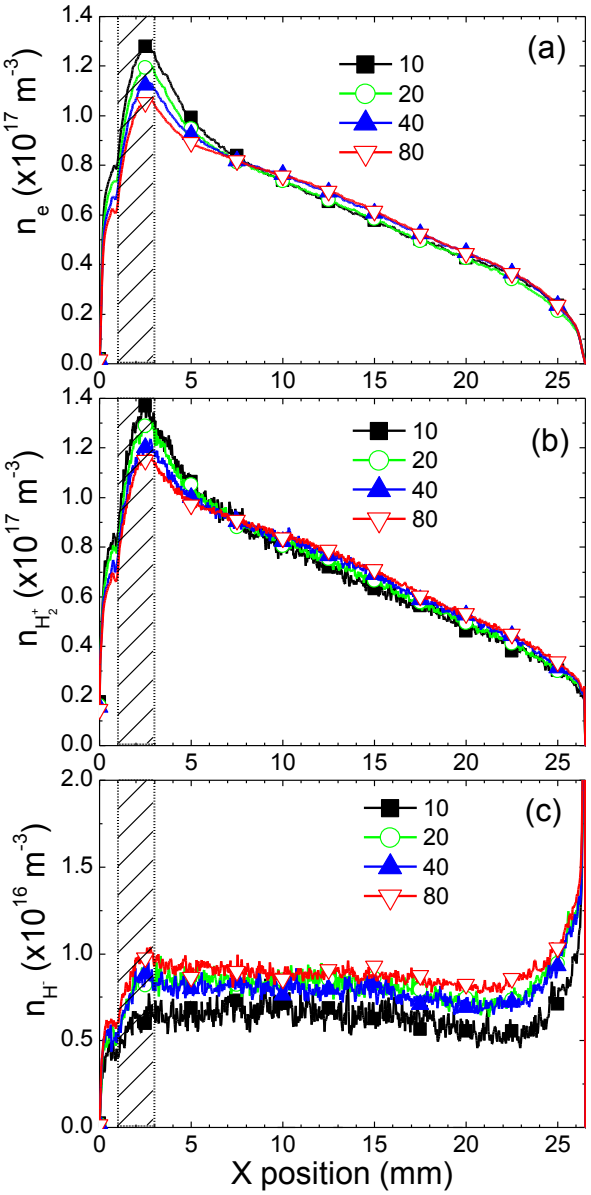
(a)
(b)
(c)
10
20
40
80
n_e (x10^{17} m^{-3})
$n_{H_2^+}$ (x10^{17} m^{-3})
n_{H^-} (x10^{16} m^{-3})
X position (mm)

Figure 7.

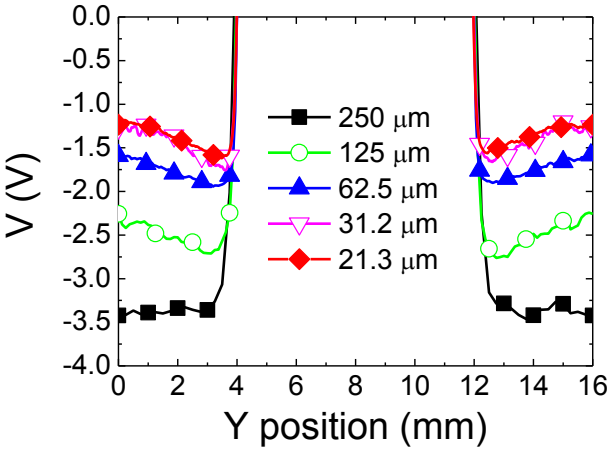
0.0
-0.5
-1.0
-1.5
-2.0
-2.5
-3.0
-3.5
-4.0
V (V)
0
2
4
6
8
10
12
14
16
Y position (mm)
250 μm
125 μm
62.5 μm
31.2 μm
21.3 μm

Figure 8.

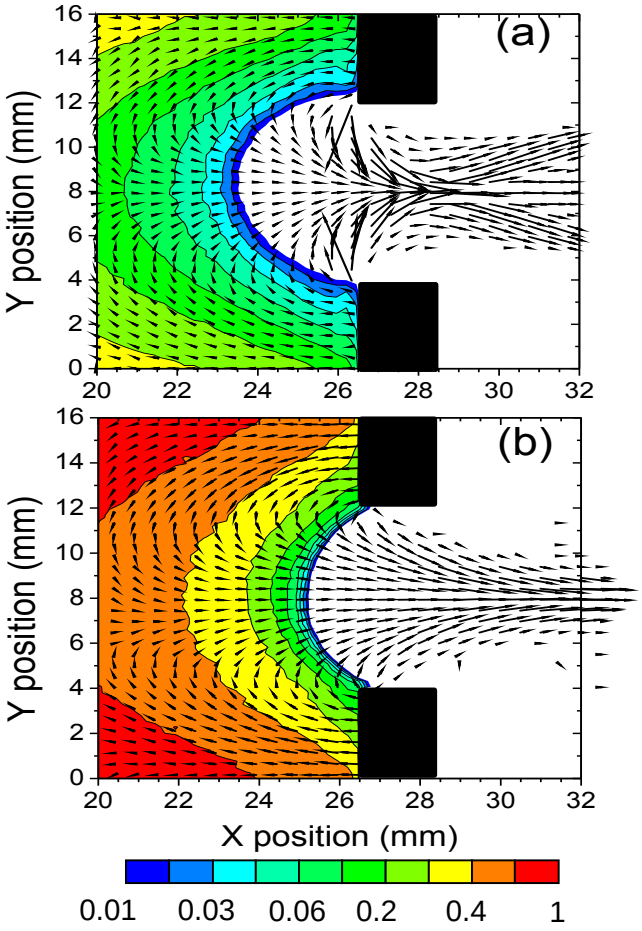
(a)
(b)
Y position (mm)
X position (mm)
0
2
4
6
8
10
12
14
16
20
22
24
26
28
30
32
0.01
0.03
0.06
0.2
0.4
1

Figure 9.

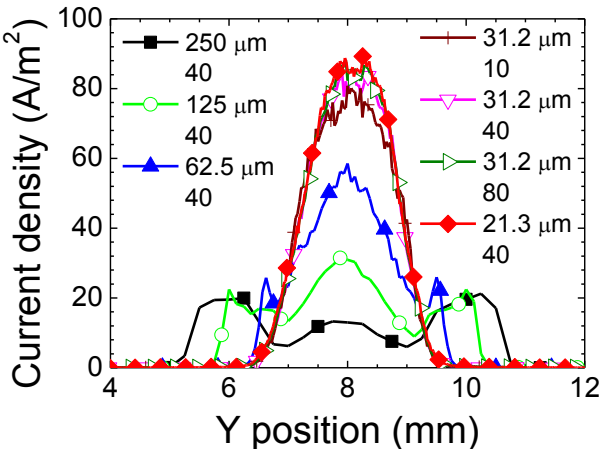
Current density (A/m^2)
Y position (mm)
250 μm
40
125 μm
40
62.5 μm
40
31.2 μm
10
31.2 μm
40
31.2 μm
80
21.3 μm
40
0
20
40
60
80
100
4
6
8
10
12

Figure 10.